# Gas Giant Protoplanets Formed by Disk Instability in Binary Star Systems

A. P. Boss

Department of Terrestrial Magnetism, Carnegie Institution of Washington, 5241 Broad Branch Road, NW, Washington, DC 20015-1305

E-mail: boss@dtm.ciw.edu

## **ABSTRACT**

Roughly half of nearby primary stars are members of binary or multiple systems, so the question of whether or not they can support the formation of planetary systems similar to our own is an important one in the search for life outside our solar system. Previous theoretical work has suggested that binary star systems might not be able to permit the formation of gas giant planets, because of the heating associated with shock fronts driven in the stars' protoplanetary disks by tidal forces during the periodic close encounters between the two stars. As a result, the disks could become too hot for icy bodies to exist, thereby preventing giant planet formation by the core accretion mechanism, and too hot for giant planets to form by the disk instability mechanism. However, gas giant planets have been discovered in orbit around a number of stars that are members of binary or triple star systems, with binary semimajor axes ranging from  $\sim 12$  to over 1000 AU. We present here a suite of three dimensional radiative gravitational hydrodynamics models suggesting that binary stars may be quite capable of forming planetary systems similar to our own. One difference between the new and previous calculations is the inclusion of artificial viscosity in the previous work, leading to significant conversion of disk kinetic energy into thermal energy in shock fronts and elsewhere. New models are presented showing how vigorous artificial viscosity can help to suppress clump formation. The new models with binary companions do not employ any explicit artificial viscosity, and also include the third (vertical) dimension in the hydrodynamic calculations, allowing for transient phases of convective cooling. The new calculations of the evolution of initially marginally gravitationally stable disks show that the presence of a binary star companion may actually help to trigger the formation of dense clumps that could become giant planets. Earth-like planets would form much later in the inner disk regions by the traditional collisional accumulation of progressively

larger, solid bodies. We also show that in models without binary companions, which begin their evolution as gravitationally stable disks, the disks evolve to form dense rings, which then break-up into self-gravitating clumps. These latter models suggest that the evolution of any self-gravitating disk with sufficient mass to form gas giant planets is likely to lead to a period of disk instability, even in the absence of a trigger such as a binary star companion.

Subject headings: solar system: formation – planetary systems – accretion, accretion disks

## 1. Introduction

Duquennoy & Mayor (1991) found that only 1/3 of the 164 G dwarf primary stars within 22 pc of the sun might be true single stars, that is, stars having no companions more massive than  $0.01~M_{\odot}$ . About 2/3 of the G dwarf primaries are thus members of binary or multiple star systems. The binary frequency for M dwarf primaries within 20 pc is somewhat lower, no more than 1/2 (Fischer & Marcy 1992). As a result, it appears that roughly half the nearby primary stars are single stars. Considering that the other half have at least one more stellar companion, less than a third of all of the nearby stars are single stars like the sun. Given the drive to detect and characterize Earth-like planets around the closest stars, it is clear that binary stars need to be as thoroughly scrutinized as single stars to see if they might also be hospitable abodes for habitable planets.

Binary stars have been included on radial velocity planet searches for quite some time, beginning with the pioneering search by Walker et al. (1995). Over 20 years of data has strengthened the case for a planet with a minimum mass of 1.7  $M_J$  (Jupiter masses) orbiting with a semimajor axis of 2.13 AU around  $\gamma$  Cephei A (Walker et al. 1992; Hatzes et al. 2003). The  $\gamma$  Cephei binary system has an orbital period of  $\sim$  57 yrs, implying an orbital separation of  $\sim$  18.5 AU (Hatzes et al. 2003). Several other binary systems with separations of  $\sim$  20 AU appear to have planetary companions, Gl 86 and HD 41004 A (Eggenberger et al. 2004). However, of the binary or multiple systems with planets detected to date, most of the systems are considerably wider, with semimajor axes ranging from  $\sim$  100 AU to  $\sim$  1000 AU or larger (Eggenberger et al. 2004; Mayor et al. 2004; Mugrauer et al. 2004; Halbwachs et al. 2005). Three of the planet host stars are members of hierarchical triple systems, HD41004 A, HD 178911 B (Zucker et al. 2002), and 16 Cygni B, with the planet orbiting the single member of the triple system. Searches are underway for unknown binary companions to planet host stars, with the consequence being that the number of planets found in binary or multiple star systems is likely to increase as more companions are detected (Patience et

al. 2002; Mugrauer et al. 2004). Currently there are at least 29 known binary or triple star systems with extrasolar planets (M. Mugrauer 2004, private communication).

Theoretical work on planet formation in binary systems has been minimal because of the decades-long focus on understanding the origin of the solar system. The discovery of extrasolar planets in binary systems has now enlarged the theoretical realm to include binary stars as well. Marzari & Scholl (2000) and Barbieri, Marzari, & Scholl (2002) modeled the formation of terrestrial planets in the  $\alpha$  Centauri binary star system, with a separation of  $\sim$ 24 AU. They found that while gravitational perturbations by the binary companion could excite the eccentricities (and hence relative velocities) of planetesimals to values high enough to halt growth, the presence of gas drag introduces an orbital phasing that minimizes their relative velocities and allow collisions to lead to growth rather than to fragmentation, at least close ( $\sim 2$  AU) to one of the binary stars. Using a symplectic integrator developed by Chambers et al. (2002), Quintana et al. (2002) modeled the final phase of growth of planetary embryos into terrestrial planets in the  $\alpha$  Centauri system, finding that multiple terrestrial planets could form, provided that the protoplanetary disk was inclined by no more than 60 degrees to the plane of the binary system. Kortenkamp, Wetherill, & Inaba (2001) found that a binary companion could serve as a source of orbital eccentricities leading to runaway growth of planetary embryos into terrestrial planets, hastening the formation process, as was also found by Quintana et al. (2002).

Moriwaki & Nakagawa (2004) extended the study of planetesimal accretion to *circumbinary* protoplanetary disks, finding that for a 1 AU binary separation and eccentricity e = 0.1, planetesimals could only grow outside of 13 AU. Nelson (2003) studied the orbital evolution of gas giant planets formed in circumbinary disks, finding that evolution can lead to either ejection of the planet or to a stable orbit. Marzari, Weidenschilling, Barbieri, & Granata (2005) studied the orbital evolution of gas giant planets orbiting one of the stars in a binary system, finding that unstable initial conditions resulted in the hyperbolic ejection of one or more planets, with the remaining planet being left behind on an eccentric, shorter-period orbit.

Thébault et al. (2004) examined the formation of  $\gamma$  Cephei's gas giant planet in the core accretion scenario (Mizuno 1980), subject to the gravitational perturbations of the binary companion on a moderately eccentric (e = 0.36) orbit. They found that with a massive gaseous disk, needed to achieve orbital phasing, a 10  $M_{\oplus}$  core could grow in  $\sim$  10 Myr, but that the core always ended up at 1.5 AU, rather than out at the observed 2.1 AU.

Nelson (2000) modeled the thermal and hydrodynamical evolution of protoplanetary disks in an equal-mass binary system with a semimajor axis of 50 AU and e = 0.3. The model was chosen to represent the L1551 IRS5 binary protostar system, where 0.05  $M_{\odot}$ 

disks orbit a pair of  $0.5~M_{\odot}$  protostars (Rodríguez et al. 1998). Nelson (2000) found that following each periastron, the disks were heated by internal shocks to such an extent that disk temperatures increased enough (to  $\sim 200~\mathrm{K}$  at 10 AU) to not only prevent gas giant planet formation by disk gravitational instability (Boss 1997), but also enough to vaporize volatile solids and thereby prevent gas giant planet formation by core accretion (Mizuno 1980). Nelson (2000) concluded that "planet formation is unlikely in equal-mass binary systems with  $a \sim 50~\mathrm{AU}$ ."

Given the existence of several gas giant planets in binary systems with separations of 20 AU or less, the negative results of Thébault et al. (2004) and Nelson (2000) regarding the formation of gas giant planets in binary systems clearly call for a re-examination of this important question. The main thrust of this paper is to present radiative hydrodynamical models of the disk instability mechanism for giant planet formation (Boss 1997, 2001, 2002a,b, 2003) that add in the effects of a binary star companion. Recent calculations with very high spatial resolution have shown that the disk instability mechanism appears to become increasingly vigorous as the continuum limit is approached (Boss 2005), and furthermore that planets formed by this mechanism are relatively immune to loss by orbital migration during a phase of gravitational instability. We shall see that disk instability appears to be capable of leading to the rapid formation of gas giant planets in binary systems with a range of semimajor axes, provided that the disk midplanes are cooled on an orbital time scale by vertical convection, as is indicated by similarly detailed models (Boss 2004a). In fact, binary companions appear to be able to stimulate the formation of self-gravitating protoplanets in otherwise stable disks.

# 2. Numerical Methods

The numerical calculations were performed with a finite volume hydrodynamics code that solves the three dimensional equations of hydrodynamics and the Poisson equation for the gravitational potential. The same code has been used in many previous studies of disk instability (Boss 2001, 2002a,b, 2003, 2004a, 2005) and has been shown to be second-order-accurate in both space and time through convergence testing (Boss & Myhill 1992). The code has been tested on a variety of test cases (Boss & Myhill 1992), including the nonisothermal test case for protostellar collapse (Myhill & Boss 1993). Bodenheimer et al. (2000) found that the results obtained with this code agreed well with those of an adaptive mesh refinement (AMR) code on isothermal collapse calculations.

The equations are solved on a spherical coordinate grid with  $N_r = 101$ ,  $N_\theta = 23$  in  $\pi/2 \ge \theta \ge 0$ , and  $N_\phi = 256$  or 512. The radial grid is uniformly spaced with  $\Delta r = 0.16$ 

AU between 4 and 20 AU. The  $\theta$  grid is compressed into the midplane to ensure adequate vertical resolution ( $\Delta\theta=0.3^{o}$  at the midplane). The  $\phi$  grid is uniformly spaced, to prevent any bias in the azimuthal direction. The central protostar wobbles in response to the growth of nonaxisymmetry in the disk, thereby preserving the location of the center of mass of the star and disk system. The number of terms in the spherical harmonic expansion for the gravitational potential of the disk is  $N_{Ylm}=32$  or 48. The Jeans length criterion (Boss 2002b) is used to ensure that the clumps that form are not numerical artifacts: even at the maximum clump densities, the numerical grid spacings in all three coordinate directions remain less than 1/4 of the local Jeans length.

The boundary conditions are chosen at both 4 and 20 AU to absorb radial velocity perturbations rather than to reflect mass and momentum back into the main grid (Boss 1998). Mass and linear or angular momentum entering the innermost shell of cells at 4 AU are added to the central protostar and thereby removed from the hydrodynamical grid. No matter is allowed to flow outward from the central cell back onto the main grid. Similarly, mass and momentum that reaches the outermost shell of cells at 20 AU piles up in this shell with zero radial velocity and is not allowed to return to the main grid. The outermost gas does however continue to exert gravitational forces on the rest of the disk.

As in Boss (2001, 2002a,b, 2003, 2004a, 2005), the models treat radiative transfer in the diffusion approximation, which should be valid near the disk midplane and throughout most of the disk, because of the high vertical optical depths. The divergence of the radiative flux term is set equal to zero in regions where the optical depth  $\tau$  drops below 10, in order to ensure that the diffusion approximation does not affect the solution in regions where it is not valid. As a result, it has not been found necessary to include a flux-limiter in the models (Boss 2001). The energy equation is solved explicitly in conservation law form, as are the four other hydrodynamic equations. Further details about the code may be found in Boss (2002b).

# 3. Artificial Viscosity

Artificial viscosity has not been used in the previous disk instability models published by Boss (2001, 2002a,b, 2003, 2004a, 2005), but it has been included in a few models presented here in order to explore its effects on clump formation. The implicit artificial viscosity of this second-order accurate code, coupled with small time steps (a result in part of the use of the spherical coordinate system, rather than cylindrical coordinates), is sufficient to maintain stability of the code even in the presence of the strong shocks driven by binary companions.

Artificial viscosity can be used to help stabilize numerical schemes and to provide microphysical heating within shocks. We use a tensor artificial viscosity (Tscharnuter & Winkler 1979), which enters into the momentum equations as follows, where the other source terms on the right hand sides of these equations are suppressed for clarity,

$$\begin{split} \frac{\partial(\rho v_r)}{\partial t} + \nabla \cdot (\rho v_r \vec{v}) &= \ldots - \frac{1}{r^3} \frac{\partial (r^3 Q_r^r)}{\partial r}, \\ \frac{\partial (\rho v_\theta)}{\partial t} + \nabla \cdot (\rho v_\theta \vec{v}) &= \ldots - \frac{1}{r sin \theta} \frac{\partial (sin \theta Q_\theta^\theta)}{\partial \theta} + \frac{Q_\phi^\phi cot \theta}{r}, \\ \frac{\partial (\rho A)}{\partial t} + \nabla \cdot (\rho A \vec{v}) &= \ldots - \frac{\partial Q_\phi^\phi}{\partial \phi}, \end{split}$$

where  $\rho$  is the mass density,  $\vec{v} = (v_r, v_\theta, v_\phi)$  is the velocity,  $A = r \sin\theta v_\phi$  is the specific angular momentum, and the  $Q_r^r$ ,  $Q_\theta^t$ , and  $Q_\phi^t$  terms are the components of the artificial viscosity tensor. The artificial viscosity tensor is set equal to zero when the divergence of the velocity field  $(\nabla \cdot \vec{v})$  is positive (i.e., in expanding regions), and when the divergence is negative, is defined to be

$$\begin{split} Q_r^r &= l_r^2 \; \rho \; \nabla \cdot \vec{v} \; (\frac{\partial v_r}{\partial r} - \frac{1}{3} \nabla \cdot \vec{v}), \\ Q_\theta^\theta &= l_\theta^2 \; \rho \; \nabla \cdot \vec{v} \; (\frac{1}{r} \frac{\partial v_\theta}{\partial \theta} + \frac{v_r}{r} - \frac{1}{3} \nabla \cdot \vec{v}), \\ Q_\phi^\phi &= l_\phi^2 \; \rho \; \nabla \cdot \vec{v} \; (\frac{1}{r sin\theta} \frac{\partial v_\phi}{\partial \phi} + \frac{v_r}{r} + \frac{v_\theta cot\theta}{r} - \frac{1}{3} \nabla \cdot \vec{v}), \end{split}$$

where  $l_r^2 = max(C_r r^2, C_{\Delta r} \Delta r^2)$ ,  $l_\theta^2 = C_\theta (r\Delta\theta)^2$ , and  $l_\phi^2 = C_\phi (rsin\theta\Delta\phi)^2$ .  $\Delta r$ ,  $\Delta \theta$ , and  $\Delta \phi$  are the local grid spacings,  $C_{\Delta r}$ ,  $C_\theta$ , and  $C_\phi$  are free parameters usually set equal to 1, and  $C_r$  is a free parameter usually set equal to  $10^{-4}$ . The contribution to the right hand side of the specific internal energy equation is then

$$E_Q = -Q_r^r \varepsilon_r^r - Q_\theta^\theta \varepsilon_\theta^\theta - Q_\phi^\phi \varepsilon_\phi^\phi$$

where

$$\varepsilon_r^r = \frac{\partial v_r}{\partial r}, \varepsilon_\theta^\theta = \frac{1}{r} \frac{\partial v_\theta}{\partial \theta} + \frac{v_r}{r}, \varepsilon_\phi^\phi = \frac{1}{r sin\theta} \frac{\partial v_\phi}{\partial \phi} + \frac{v_r}{r} + \frac{v_\theta cot\theta}{r}.$$

 $E_Q$  is constrained to be positive or zero, reflecting the role of the artificial viscosity as a dissipative mechanism. When artificial viscosity is to be used, the coefficient  $C_{\phi}$  normally is set equal to zero in order to preserve the local conservation of angular momentum. Only selected terms from the complete tensor have been employed here. Terms involving coupling the r and  $\theta$  components with the  $\phi$  components have been dropped (i.e.,  $Q_{\phi}^{r}$ ,  $Q_{\phi}^{\phi}$ , and  $Q_{\theta}^{\phi}$  are neglected), in order to conserve angular momentum locally in a consistent manner (see test cases in Boss & Myhill 1992).

#### 4. Initial Conditions

The standard model consists of a  $1M_{\odot}$  central protostar surrounded by a disk with a mass of 0.091  $M_{\odot}$  between 4 and 20 AU. Disks with similar masses appear to be necessary to form gas giant planets by core accretion (e.g., Inaba, Wetherill, & Ikoma 2003). Most models also include the gravitational forces associated with a  $1M_{\odot}$  binary star companion, as described below. Note that the initial disk model does not include the gravitational forces from the binary companion, so the evolution proceeds as if the binary companion has just been formed, an unrealistic but necessary assumption that is needed in order to make progress on this problem.

# 4.1. Disk density

The initial protoplanetary disk structure is based on the following approximate vertical density distribution (Boss 1993) for an adiabatic, self-gravitating disk of arbitrary thickness in near-Keplerian rotation about a point mass  $M_s$ 

$$\rho(R,Z)^{\gamma-1} = \rho_0(R)^{\gamma-1}$$
$$-\left(\frac{\gamma-1}{\gamma}\right) \left[ \left(\frac{2\pi G\sigma(R)}{K}\right) Z + \frac{GM_s}{K} \left(\frac{1}{R} - \frac{1}{(R^2 + Z^2)^{1/2}}\right) \right],$$

where R and Z are cylindrical coordinates,  $\rho_0(R)$  is the midplane density, G is the gravitational constant, and  $\sigma(R)$  is the surface density. For setting up the initial model only,  $K = 1.7 \times 10^{17}$  (cgs units) and  $\gamma = 5/3$ . The radial variation of the midplane density is

$$\rho_0(R) = \rho_{04} \left(\frac{R_4}{R}\right)^{3/2},$$

where  $\rho_{04} = 1.0 \times 10^{-10} \text{ g cm}^{-3} \text{ and } R_4 = 4 \text{ AU}.$ 

## 4.2. Disk temperatures

The initial temperature profile is based on two dimensional radiative hydrodynamics calculations (Boss 1996) and is the same as was used in previous models (Boss 2001, 2002a,b, 2004a). A range of outer disk temperatures are investigated, with  $T_o = 40, 50, 60, 70, \text{ or}$ 80 K (Table 1). As a result of the initial temperature and density profiles, the initial disks have Q gravitational stability parameters whose minima range from  $Q_{min} = 1.3$  for  $T_o = 40$ K. to  $Q_{min} = 1.9$  for  $T_o = 80$ K. [Q is defined to be  $Q = c_s \Omega/(\pi G \sigma)$ , where  $c_s$  is the isothermal sound speed,  $\Omega$  is the angular velocity, and  $\sigma$  is the surface mass density of the disk.  $T_o = 80$ K is considerably higher than the temperatures at which the solar system's comets are thought to have formed – the experiments of Notesco & Bar-Nun (2005) imply that cometary nuclei agglomerated from dust grains at  $\sim 25$  K, while observations of nuclear spin temperatures of H<sub>2</sub>O in three Oort Cloud comets suggest formation temperatures of  $\sim 20$  to  $\sim 45$  K (Dello Russo et al. 2005). The Oort Cloud comets are thought to have formed between 5 and 40 AU, so they provide the ground truth for theoretical models of giant planet formation, at least in our planetary system. The outer disk temperatures of 60, 70, and 80 K were then purposely chosen to be higher than expected for the solar nebula, in order to err on the conservative side with regard to the outcome of a phase of disk instability. Alternatively, models could be run with outer disk temperatures closer to those inferred from comets, but with lower disk masses, so that the initial values of Q are again well above  $\sim$ 1.5, implying a relatively gravitationally stable initial disk. Models starting with the same Q values should evolve very similarly.

In low optical depth regions, such as in the envelope infalling onto the disk, the temperature is assumed to be 50 K in the models, consistent with heating by radiation at distances of order 10 AU from a quiescent, solar-mass protostar (Chick & Cassen 1997). I.e., the disk surface is assumed to be immersed in a thermal bath at a temperature of 50 K; the outer layers of the disk are thus assumed to be able to radiate at whatever temperature is needed to maintain this gas temperature. A more detailed calculation of the thermal structure at the disk surface should be explored in future models, as the surface temperature throttles disk cooling. E.g., Chiang et al. (2001) calculated radiative, hydrostatic equilibrium models of flared protoplanetary disks heated by radiation from their central stars. Their two-layer disk models consisted of a disk surface and a disk interior, with the optically thin disk surface being hotter than the disk interior, given the assumed heat source. At a distance of 10 AU in their standard model, the disk surface temperature is  $\sim 100 \text{ K}$  and the interior temperature

is  $\sim 50$  K. While the gas and dust temperatures are roughly equal inside the disk, well above the disk's photosphere the gas temperature can reach temperatures of  $\sim 10^4$  K (Kamp & Dullemond 2004). Mechanical heating associated with dynamical processes in the disk midplane may be the source of the superheated atmospheres inferred for inner protoplanetary disks (Glassgold, Najita, & Igea 2004). At distances of 50 AU or more, observations imply a vertical temperature gradient, with midplane temperatures of  $\sim 13$ -20 K underlying outer layers with temperatures of  $\sim 30$  K (Dartois, Dutrey, & Guilloteau 2003).

## 5. Binary Star Companion

The binary models include the gravitational accelerations from a binary star companion to the solar-mass star around that the disk orbits. The models neglect any radiation coming from the second star in the system.

#### 5.1. Tidal Potential

The tidal potential at a position  $\vec{r}$  due to a binary star companion with mass  $M_b$  located at  $\vec{r_b}$  is given by

$$\Phi_{tide}(\vec{r}) = -\frac{GM_b}{|\vec{r} - \vec{r_b}|},$$

where the binary star companion is represented as a single point mass. The tidal potential may then be expressed in terms of an expansion in Legendre polynomials  $P_l$  of order l as

$$\Phi_{tide}(\vec{r}) = -\frac{GM_b}{r_b} \sum_{l=0}^{\infty} \left(\frac{r}{r_b}\right)^l P_l(cosS),$$

where S is the angle between  $\vec{r}$  and  $\vec{r}_b$ . The l=1 term in this expansion is responsible for the acceleration of the primary star and its disk toward the binary companion, an acceleration that is balanced by the centrifugal force necessary for orbital motion of the primary star and its disk around the center of mass of the entire system. Hence we take as the tidal potential the following

$$\bar{\Phi}_{tide}(\vec{r}) = -\frac{GM_b}{|\vec{r} - \vec{r_b}|} + \frac{GM_br}{r_b^2} cosS.$$

The first non-trivial term in the tidal potential expansion will then be the l=2 term, which forces the disk into a prolate-ellipsoidal shape. When  $\bar{\Phi}_{tide}(\vec{r})$  is added into the gravitational potential of the disk, obtained from the solution of Poisson's equation, we have effectively included the tidal force of the orbiting binary companion (Boss 1981) as well as the orbital motion of the star/disk around the center of mass of the entire system. No other changes are needed for the equations of motion (Mizuno & Boss 1985).

# 5.2. Binary Star Orbit

We employ a nonrotating, noninertial reference frame for the models with a binary star companion, with the coordinate origin fixed at the center of mass of the primary star and its disk. Because of the way that the tidal force of the binary companion has been included, in this reference frame the binary companion appears to orbit around the coordinate origin of the disk whose evolution is being calculated (Mizuno & Boss 1985). A similar approach was used by Larwood et al. (1996) in their models of accretion disks being warped by binary companions. In the present models, the binary star is assumed to lie in the same plane as the disk, so that no warps are created, and the disk retains its symmetry above and below its midplane.

The binary star companion is assumed to be on an orbit with eccentricity  $e_b$  and semimajor axis  $a_b$  (Table 1).  $\phi_{bi}$  defines the initial position angle of the binary in its eccentric orbit, with  $\phi_{bi} = 0$  corresponding to starting at periastron, and  $\phi_{bi} = \pi$  to apoastron.  $\phi_b(t)$ denotes the position angle of the companion as it moves along its orbit (i.e., the true anomaly, f). For Keplerian orbits,  $\phi_b(t)$  is calculated by

$$\phi_b(t) = \phi_{bi} + \int_0^t \left[ \frac{J_b}{r_b^2(t)} \right] dt,$$

where the angular momentum per unit mass  $J_b$ , a constant, is equal to

$$J_b = \Omega_b a_b^2 (1 - e_b^2)^{1/2}$$
.

 $\Omega_b$ , the mean motion, is equal to  $\Omega_b = 2\pi/P_b$ , where  $P_b$  is the orbital period of the binary. The mean motion is also equal to

$$\Omega_b = \left(\frac{G(M_s + M_b)}{a_b^3}\right)^{1/2},$$

where  $M_s$  is the mass of the star with the disk. The binary separation  $r_b(t)$  is determined from the time evolution of  $\phi_b(t)$  through

$$r_b(t) = a_b \frac{(1 - e_b^2)}{(1 + e_b \cos \phi_b(t))}.$$

In these models, an equal mass binary system is assumed, i.e.,  $M_s = M_b = 1M_{\odot}$ . The only free parameters then are  $a_b$ ,  $e_b$ , and  $\phi_{bi}$ , as noted in Table 1. Models with  $\phi_{bi} = 0$  start at periastron, so that  $r_b(t=0) = a_b(1-e_b)$ , whereas models with  $\phi_{bi} = \pi$  start at apoastron, so that  $r_b(t=0) = a_b(1+e_b)$ . In order to avoid abrupt initial changes in the disk when starting a model, the tidal forces begin at zero strength and increase linearly with time over the first 30 yrs of evolution, when their full strength is reached and maintained thereafter.

## 6. Results

Table 1 summarizes the disk models with and without binary companions. The latter models are presented here in order to be able to separate out the effects of including the binary companions from what the disks would do in the absence of external forces.

#### 6.1. Models without Binary Companions

We begin with several disk instability models that are identical to those previously published by Boss (2002), except for starting with higher initial outer disk temperatures ( $T_o$ ). Boss (2002) presented results for models with initial  $T_o = 40 \,\mathrm{K}$  and 50 K (as in models eb and ab), leading to initial Toomre (1964) Q stability values of  $Q_{min} = 1.3$  and 1.5, respectively. In these initially marginally gravitationally unstable disks, strongly nonaxisymmtric structures begin to form within a few hundred years of evolution, equal to about 10 orbital periods at an orbital radius of  $\sim 10 \,\mathrm{AU}$  where clumps first appear in an unperturbed disk of this type. Given that the orbital period of the  $a_b = 50 \,\mathrm{AU}$  binary system is 250 yrs, it is clear that the unperturbed disks with initial  $Q_{min} = 1.3$  and 1.5 can be expected to develop nonaxisymmetry on the same time scale as the binary perturbations. Hence models were studied with higher initial temperatures in order to try to see what would happen in a disk that might not do much on its own prior to being excited by the binary perturber. Models f, g, and h thus began with  $T_o = 60 \,\mathrm{K}$ , 70 K, and 80 K, respectively, leading to an initial  $Q_{min} = 1.6$ , 1.8, and 1.9. These models are more gravitationally stable initially than models with  $T_o = 40 \,\mathrm{K}$  and 50 K, and hence should also represent a protoplanetary disk that has not yet

evolved into a state of marginal gravitational instability.

Figure 1 shows the initial radial distribution of the surface density in model f with  $T_o =$ 60K, compared to the critical surface density needed to make the disk have a Toomre Q=1at that radius, i.e., in order to be strongly gravitationally unstable initially. Because the initial temperature profile rises high above  $T_o$  inside  $\sim 8$  AU, this critical surface density rises sharply as well. Hence the innermost regions are expected to remain gravitationally stable. Figure 2 shows the surface density for model f after 87.1 yrs of evolution. The presence of axisymmetric rings and growing spiral arms can be inferred from the ripples in the surface density. In addition, it is clear that the region inside  $\sim 6$  AU has already been significantly modified from the initial profile, with mass having been transported inward onto the central protostar as well as outward to the growing ring centered around 6 AU. Figures 3 and 4 show the further evolution of model f after 160 yrs and 233 yrs, respectively, as the innermost region is severely depleted of gas and dense ring-like features grow between 8 AU and 10 AU. The high average surface density at the 4 AU inner boundary is produced by a few dense cells where disk mass is flowing onto the central protostar and exiting the hydro grid. These figures show that the disk evolves to form rings that become increasingly closer to Toomre Q=1 instability [in fact, the Toomre (1964) criterion explicitly refers to ring formation as a predecessor to the development of nonaxisymmetry.

This trend is further displayed in Figures 5 and 6, which show the evolution of the Toomre Q parameter for model h ( $T_o = 80$  K). Starting from a disk with a minimum Toomre Q value of 1.9, considerably stabler than model f with 1.6, Figure 6 shows that after 245 yrs of evolution the disk has formed rings around 10 AU where Q drops to  $\sim 1.5$ , sufficient for marginal gravitational instability. The inner regions become even more stable (Q > 2) as a result of their higher temperatures and depleted gas surface density. Figures 1-6 make it clear why clumps tend to form preferentially around 10 AU in these models, as interior to that distance is where midplane temperatures rise to higher values at smaller radii and where the disk surface density is depleted by accretion onto the central protostar. Beyond 10 AU the instability proceeds somewhat slower because of the longer orbital time periods.

Figures 7 and 8 show the formation of clumps in models f and h at times of 233 yrs and 245 yrs, respectively. While the clumps are not necessarily self-gravitating at this phase of evolution, it is clear that these disks are trying to form clumps in spite of their relatively high initial outer disk temperatures, higher in fact than appears to be appropriate for the solar nebula based on cometary speciation (e.g., Dello Russo et al. 2005).

Evidently even low amplitude nonaxisymmetry can transfer mass and angular momentum over times of order 10 orbital periods sufficient to approach a more robust phase of gravitational instability. Models f, g, and h suggest that the natural evolution of gravi-

tationally stable disks is toward marginal gravitational instability and then on to clump formation, even in the absence of triggering effects such as binary companions or secular cooling. Note that in all of these models the outer disk temperature is not allowed to drop below the initial value of  $T_o$ , in an attempt to err on the side of being conservative with respect to thermal decompression and cooling.

# 6.2. Models with Binary Companions

Table 1 lists final times  $t_f$  of the models with binary star companions on orbits with eccentricity  $e_b$  and semimajor axis  $a_b$ . For models with  $a_b = 50$  AU, the binary orbital period is 250 yrs, while for  $a_b = 100$  AU, it is 707 yrs (note that the binary companion is also a solar-mass star). The evolution of the models following the first periastron passage of the binary companion should also be relevant for the problem of a disk around a single star that undergoes a very close encounter with another star in the star-forming cluster.

Figures 9-12 show the time evolution of model gbca, where the binary companion has  $a_b = 50$  AU and  $e_b = 0.5$ . The disk models start out essentially axisymmetric with only a low level ( $\sim 1\%$ ) of noise. After 83.8 yrs of evolution, the disk has become slightly nonaxisymmetric (Figure 10), primarily as a result of its own evolution (see previous section). However, by 139 yrs (Figure 11), the binary companion has completed just over half of an orbital period and has passed periastron at a distance of 25 AU from the center of the disk, severely distorting the outer regions of the disk (note that the density concentrations at 20 AU are an artifact of the disk boundary conditions at 20 AU, where disk material is allowed to enter the outermost shell of cells but cannot flow farther away as it would in a calculation with a more distant outer boundary.) The binary companion is located at this time at about 2 o'clock. Periastron was at 3 o'clock, and the binary companion orbits in a counter-clockwise sense, in the same direction that the disk gas orbits, consistent with formation of the entire system from a single rotating, dense cloud core.

While the structures in the outermost disk are strongly influenced by the outer boundary conditions, the innermost arcs are not. The tidal forces of the binary companion have forced the disk into a prolate shape that is beginning to wind-up in the inner regions because of Keplerian rotation (Figure 11). By the time of Figure 12, at 191 yrs, the binary companion is approaching apoastron, but the tidally perturbed disk is still forming spiral arms and clumps, as well as strong shock fronts in its innermost regions. Clearly the presence of a binary companion with these orbital parameters has had a major effect on the evolution of this initially gravitationally stable disk, inducing the formation of clumps after the first periastron. This fact makes it clear that starting this model with an axisymmetric disk is

not correct – in a real disk orbiting a protostar in a binary system of this type, the outer disk is never axisymmetric. Axisymmetric initial models are a theoretical convenience that allows one to jump into the system in an approximate manner and to follow the subsequent evolution.

Figure 13 shows the midplane density contours for model ab after 159 yrs. The disk has already been tidally perturbed because this model began with the binary companion at periastron, though the tidal forces were turned on over a time period of 30 yrs. A well-defined clump is evident at 6 o'clock in Figure 13, containing  $\sim 1.5 M_{Jup}$  of gas and dust. This clump is sufficiently massive to be gravitationally bound, as the Jeans mass at the mean density  $(7.2 \times 10^{-10} \text{ g cm}^{-3})$  and temperature (161 K) of this clump is only 1.4  $M_{Jup}$ . The spherically-averaged radius of the clump is 0.66 AU, only slightly larger than the tidal stability radius of 0.64 AU, implying marginal tidal stability. The clump is moving on an orbit with a=8.2 AU and e=0.094 at this time.

Figure 14 demonstrates that the clump in Figure 13 is properly resolved with respect to the Jeans length criterion, which dips to close to the grid resolution at the location of the clump's density maximum, seen in Figure 15. Figure 16 shows how the temperatures within the clump have risen considerably over the initial temperatures as a result of compressional heating – the maximum temperature in the clump exceeds 300 K, compared to a mean temperature of 161 K. Figure 17 shows the temperature distribution thoughout the midplane of model ab after 159 yrs, showing the effects of heating throughout the disk. The disk is vertically unstable to convection according to the Schwarzschild criterion at the location of the dense clump seen in Figure 13, as well as at a number of other radii near the midplane in model ab. Convective cooling appears to be important for transporting thermal energy from the disk midplane to the disk atmosphere, where it can be radiated away, allowing a disk instability to produce dense clumps centered on the midplane (Boss 2004a).

The effect of the binary eccentricity on the models can be seen by comparing Figures 18 and 19. Models hbcae (Figure 18) and hbca (Figure 19) are identical except that the binary eccentricity is 0.25 for the former and 0.5 for the latter ( $a_b = 50$  AU for both models). As a consequence, periastron occurs at a radius of 37.5 AU for model hbcae and at 25 AU for model hbca, leading to considerably stronger tidal forces in the latter model. Figures 18 and 18 demonstrate this point after one binary orbital period has elapsed: while both disks have formed strong spiral arms and clumps, model hbca is clearly more strongly distorted and has developed higher densities along the outer boundary of the disk. The clump at 10 o'clock in Figure 18 has a mass of 4.7  $M_{Jup}$ , sufficiently high to be strongly self-gravitating, whereas the clump at 2 o'clock in Figure 19 is not quite self-gravitating with a mass of 0.68  $M_{Jup}$ . This suggests that while binary perturbers can stimulate clump formation, too strong

of a perturbation can make it harder for the clumps to survive to become true protoplanets. However, even in model hbca, other clumps form later in the evolution that are dense enough and massive enough to be self-gravitating.

The effect of the binary semimajor axis on the models can be seen by comparing Figures 20 and 21. Models gba (Figure 20) and gbca (Figure 21) are identical except that the semimajor axis is 100 AU for the former and 50 AU for the latter ( $e_b = 0.5$  AU for both models). As a consequence, periastron occurs at a radius of 50 AU for model gba and at 25 AU for model gbca, again leading to considerably stronger tidal forces in the latter model. Figures 20 and 21 demonstrate the effects of these different semimajor axes, shortly after one binary orbital period has elapsed, in order to compare these models at an equivalent time with respect to the effects of the tidal forces. While model gba has evolved and formed spiral arms, dense clumps have not formed at this time. The evolution is closer to that of the disk models without binary companions – evidently tidal forces from binary companions at distances of  $\sim 50$  AU or greater have relatively little effect on the disk inside 20 AU. In model gbca (Figure 21), on the other hand, the binary's periastron of 25 AU has had a major effect on the disk, and has induced the formation of a dense clump at 9 o'clock with a mass of 1.7  $M_{Jup}$ . Strong spiral arms are also evident throughout the disk.

In order to ascertain the effects of the numerical resolution, model gbca was continued from the time shown in Figure 21 as model gbcah with double the number of azimuthal grid points (i.e.,  $N_{\phi} = 512$  instead of  $N_{\phi} = 256$ ), and more terms in the gravitational potential solution (i.e.,  $N_{Ylm} = 48$  instead of  $N_{Ylm} = 32$ ). Model gbcah is shown in Figure 22 after another 28 yrs of evolution beyond the point shown in Figure 21, i.e., roughly another orbital period at  $\sim 10$  AU. A self-gravitating clump orbits at 10 AU (seen at 8 o'clock) with a mass of 1.2  $M_{Jup}$ , well above the relevant Jeans mass of 0.72  $M_{Jup}$ , with a radius (0.76 AU) comparable to the tidal stability radius (0.75 AU). Clump formation and survival is enhanced as the spatial resolution is increased in the critical azimuthal direction (Boss 2000, 2005).

## 6.3. Models with Varied Thermodynamical Stability Handling

Two approaches have been used in these models and in the previous disk instability models by Boss (2001, 2002a,b, 2003, 2005) for stability of the radiative transfer solution, given the use of an explicit time differencing scheme for the solution of the energy equation in the diffusion approximation. First, taking smaller time steps (i.e., smaller fractions of the Courant time) is often sufficient to maintain stability of the thermodynamical solution. The calculations typically begin with a time step that is 50% of the minimum Courant

time on the grid. For some models, this fraction is reduced to maintain stability, to values as small as 1%, though typically the fraction remains no smaller than 5% or 10%. While sufficient to maintain stability, clearly this approach slows the calculation proportionately. Hence it has been found useful to use a numerical artifice to try to maintain stability of the numerical solution of the energy equation in the low density regions where it tends to break down. The artifice is simple: when the density inside the disk drops below a specified critical value,  $\rho_{crit}$ , then the temperature in that cell is forced back to its initial temperature at the beginning of the evolution. This artifice is justified to the extent that such regions are low in density because they are undergoing decompression, and hence should also be undergoing decompressional cooling. Setting the temperatures of such regions to a value no lower than their initial temperature is then a relatively conservative approach.

While the question of the handling of  $\rho_{crit}$  may seem to be largely a technical point, given the sensitivity of the outcomes of disk instability calculations to the heating and cooling processes in the disk, it is important to examine any technical details that might have an unintended effect on the results.

All the models began with  $\rho_{crit}=10^{-13}~{\rm g~cm^{-3}}$ , compared to the initial midplane density of  $10^{-10}~{\rm g~cm^{-3}}$  at 4 AU. In order to maintain stability with a reasonably-sized time step, however, in some models  $\rho_{crit}$  is increased to values of  $3\times10^{-12}~{\rm g~cm^{-3}}$  or  $10^{-11}~{\rm g~cm^{-3}}$ . With these values, even moderately low density regions of the disk are effectively forced to behave isothermally. With this in mind, all the models were searched for evidence that the highest value of  $\rho_{crit}$  used had a significant effect on the outcome of the evolution. The primary criterion employed was looking for the maximum density produced in the disk midplane around 5 AU to 10 AU, where the dense clumps form. It was found that the maximum density reached was typically the same ( $\sim 2\times10^{-9}~{\rm g~cm^{-3}}$ ) independent of whether  $\rho_{crit}$  stayed at a value of  $10^{-13}~{\rm g~cm^{-3}}$  throughout the calculation, or had to be increased at some point to  $3\times10^{-12}~{\rm g~cm^{-3}}$  or  $10^{-11}~{\rm g~cm^{-3}}$  to maintain a stable solution. This results suggests that the  $\rho_{crit}$  artifice is not a major determinant of the outcome.

## 6.4. Models with Artificial Viscosity

Hydrodynamical calculations where artificial viscosity is employed generally have not found robust clump formation in either fully three dimensional (Pickett et al. 2000) or in thin disk models (Nelson 2000). Here we show that when artificial viscosity is included in three dimensional disk models with radiative and convective cooling, the tendency to form clumps is reduced somewhat, but not eliminated, unless the artificial viscosity is increased by a factor of order ten.

These models have the standard spatial resolution (Boss 2002b) of 100 radial grid points distributed uniformly between 4 and 20 AU, 256 azimuthal grid points, 22 theta grid points in a hemisphere (effectively over a million grid points), and include terms up to l, m = 32 in the spherical harmonic solution for the gravitational potential. The models begin after 322 years of inviscid evolution of a disk with an initial mass of 0.091  $M_{\odot}$  (Boss 2002b), an outer disk temperature of 40 K, and a minimum Toomre Q = 1.3.

Figures 23 through 26 show the results for four models that are identical except for their treatment of artificial viscosity. It can be seen that in the models with the standard artificial viscosity (Figure 24:  $C_{\Delta r} = C_{\theta} = 1$ ,  $C_{\phi} = 0$ ,  $C_r = 10^{-4}$ ; Figure 25: same as Figure 24, but with  $C_{\phi} = 1$ ), clump formation occurs in a similar manner as in the model without artificial viscosity (Figure 23, as in Boss 2002b). However, when the artificial viscosity is increased by a factor of 10 (Figure 26), clump formation is significantly inhibited because of the heating associated with the assumed dissipation. These models support the suggestion that microphysical shock heating can be important for clump formation (Pickett et al. 2000), though with the standard amount of artificial viscosity, the effects are relatively minor in these models. Calibrating the proper amount of artificial viscosity that would be needed to properly represent the correct level of microphysical (sub-grid) shock heating remains as a challenge, but it is clear that large amounts of artificial viscosity can suppress clump formation.

#### 7. Discussion

## 7.1. HD 188753 triple star system

Recently Konacki (2005) has claimed the discovery of a hot Jupiter in orbit around a  $1.06~M_{\odot}$  star that is a member of the hierarchical triple star system HD 188753. The average distance between the primary star and the binary secondary is 12.3 AU, with the secondary being on an orbit with e=0.5 and having a total mass of  $1.63~M_{\odot}$ . This means that at periastron, the secondary passes within  $\sim 6~{\rm AU}$  of the primary, rendering orbits outside of  $\sim 1.5~{\rm AU}$  unstable. Hot Jupiters are thought to form at several AU from solar-mass stars and then to migrate inward to short-period orbits by gravitational interactions with the gaseous disk. However, the protoplanetary disk around the primary star in HD 188753 would be restricted in extent to  $\sim 1.5~{\rm AU}$  and so could not extend out to regions cool enough for icy grains to contribute to assembling the solid core required for the core accretion mechanism or cool enough for a disk instability to occur. Given the difficulty of forming gas giant planets in situ on short period orbits by either core accretion (Bodenheimer, Hubickyj, & Lissauer 2000) or disk instability (Boss 1997), the presence of the planet in HD 188753 is

thus puzzling, given the current orbital configuration, if the discovery can be confirmed.

However, the fact that HD 188753 is a triple system offers a possible solution. Hierarchical triples can form by the orbital evolution of an initially equally-spaced multiple protostar system (e.g., Boss 2000). This evolution proceeds over a period of  $\sim$  100 orbital crossing periods. For a multiple protostar system with an initial separation of  $\sim$  100 AU, the initial orbital period would be  $\sim$  10³ yrs, so that the initial equally-spaced multiple protostar system would be expected to undergo a series of close encounters and ejections leading to the final, stable, hierarchical triple system within a time period of  $\sim$  10⁵ yrs. If a gas giant planet could form within the protoplanetary disk of one of the protostars within  $\sim$  10⁵ yrs, it might then survive the subsequent orbital evolution as a hot Jupiter. Rapid formation is required, suggesting that a disk instability might be needed to explain HD 188753's putative hot Jupiter.

#### 7.2. Previous calculations

Contrary to the results of Nelson (2000), these models suggest that tidal forces from binary companions need not prevent the formation of giant planets, by either the disk instability or core accretion mechanisms. The key difference is in the midplane temperatures reached after periastrons, with the Nelson (2000) models reaching temperatures high enough to sublimate icy dust grains at  $\sim 10$  AU and to prevent a robust disk instability inside this radius. Here we try to understand why the present results differ from those of Nelson (2000).

There are several important similarities and differences between the two sets of calculations. Nelson (2000) used 60,000 SPH (smoothed particle hydrodynamics) particles in each disk, compared to effectively over  $10^6$  grid points in the present models with  $N_{\phi}=256$ , though because Nelson's calculations were restricted to two dimensional (thin) disks, the spatial resolution was similar to that in the midplane of the present models with  $N_{\phi}=512$ . Nelson (2000) assumed a thin disk with an adiabatic vertical temperature gradient, which assumes that vertical convection is able to keep the vertical temperature gradient at the adiabatic level. This results in the maximum possible temperature difference between the disk surface (excluding the disk photosphere) and the midplane, because if radiative transport were efficient, the vertical temperature gradient would not be as steep. The present models start out vertically isothermal, but then develop vertical convective motions in regions where the vertical temperature gradient exceeds the adiabatic value (i.e., the Schwarzschild criterion for convection is met; Boss 2004a). Nelson (2000) also used disk surface temperatures (100 K) greater than those assumed in the present models (50 K), leading to higher midplane temperatures, though the higher surface temperatures should lead to a higher rate

of radiative cooling.

Perhaps the most likely source of the discrepancy is the amount of artificial viscosity assumed in the two sets of models. Artificial viscosity equivalent to an effective alpha viscosity with  $\alpha = 0.002$  to 0.005 was intentionally included in the Nelson (2000) models in an effort to include the effects of shocks and sub-grid turbulence. In the present models, artificial viscosity is not used, and the degree of implicit numerical viscosity appears to be at a level equivalent to  $\alpha \sim 10^{-4}$  (Boss 2004b), a factor of 20 to 50 times lower than that in Nelson (2000). As we have seen in Figures 23-26, a high level of artificial viscosity can heat the disk sufficiently to suppress the formation of clumps, though Figures 24 and 25 show that with a standard amount of artificial viscosity, clumps can still form. The artificial viscosity employed in SPH codes can lead to a "large and unphysical shear dissipation as a side effect in disk simulations" (Nelson et al. 2000), though Nelson et al. (2000) and Nelson (2000) used a formulation that was intended to minimize artificial viscous dissipation. Nevertheless, the intentional use of a relatively large amount of artificial viscosity (in order to attempt to duplicate spectral energy distributions for observed disks) is likely to be the main source of the discrepancy between the models. This artificial viscous heating appears to be related to the difference in cooling times in the two sets of models, as the cooling time is critical for clump formation and survival. Relatively short cooling times are obtained in the present models ( $\sim 1$  to 2 orbital periods, Boss 2004a), compared to the effective cooling time obtained in Nelson (2000) of  $\sim 5$  to  $\sim 15$  orbital periods for distances from 10 AU to 5 AU, respectively (Nelson 2005, private communication).

One could reasonably ask whether the present models are able to handle strong shocks properly in the absence of artificial viscosity, as that is how these models have been run, with the exception of the models shown in Figures 24-26. In order to test this possibility, one dimensional shock tests performed with the same hydrodynamic scheme as used in the present models and first presented by Boss & Myhill (1992) were repeated with and without artificial viscosity. The shock test relies on the analytic solution for the Burgers equation presented by Harten & Zwas (1972). Using the same numerical code and numerical parameters as presented in Figure 7 of Boss & Myhill (1992), Figures 27 and 28 depict the results with the standard amount of artificial viscosity  $(C_Q = 1)$  and with zero artificial viscosity, respectively. It can be seen that in both cases, the numerical solution does an excellent job of reproducing the analytical solution, including the shock front location. Figure 28 shows that in the complete absence of artificial viscosity, there is a similar degree of overshoot/undershoot immediately downstream of the shock front as in Figure 27 with nonzero artificial viscosity (in both cases, the overshoot/undershoot is minimal compared to that of several other differencing schemes; see Figure 7 of Boss & Myhill 1992). These results suggest that the present models, even with zero artificial viscosity, are able to handle strong shocks about as well as if the standard amount of artificial viscosity were being employed. It is thus likely that with the standard amount of artificial viscosity, the effective  $\alpha$  of the models is similar to that caused by the implicit numerical viscosity ( $\alpha \sim 10^{-4}$ ; Boss 2004b). In that case, the Nelson (2000) models effectively include viscous dissipation at a rate roughly 20 to 50 times higher than the present models, which appears to be sufficient to explain the suppression of clump formation in the Nelson (2000) models, based on the results presented in Figures 23-26.

There may be a related discrepancy between these models and those of Nelson (2000). Nelson (2000) found that the long-wavelength flux densities from his disk models were below those measured for the L1551 IRS5 binary disk system upon which his models were based, implying effective temperatures for the disk surface that were too low. However, Boss & Yorke (1993, 1996) found that they were able to match the spectral energy distributions of the T Tauri system with the same axisymmetric disk models that form the basis for the three dimensional disk models used in the present models. It is unclear at present what this means, but suffice it to say that a higher effective temperature at the disk surface should increase radiative losses from the disk surface and thereby reduce the overall disk cooling time, though perhaps at the expense of higher midplane temperatures.

#### 8. Conclusions

These models have shown that initially stable protoplanetary disks can evolve over time periods of  $\sim 10^3$  yrs to become marginally gravitationally unstable and then begin to form clumps. When these stable disks are perturbed by strong tidal forces (i.e., periastrons less than  $\sim 50$  AU), spiral arms form soon after peristron and typically evolve into selfgravitating, dense clumps capable of forming gas giant planets. Periastrons of  $\sim 50~\mathrm{AU}$ and larger lead to little effect on the evolution of these disks, which are limited in extent to 20 AU. Disk cooling processes such as convection appear to remain effective enough to permit self-gravitating clumps to form, even in the presence of the strong tidal forcing. As a result, outer disk temperatures do not become high enough in general for icy dust grains to be sublimated, meaning that giant planet formation by core accretion would continue to be aided by the enhanced surface density of solids associated with the ice condensation boundary in the disk, even in binary star systems. Given the tendency for these disks to form self-gravitating clumps by disk instability on a time scale of  $\sim 10^3$  yrs or less, these models suggest that giant planets should be able to form in binary systems with periastrons as small as 25 AU, by either core accretion or disk instability. This general conclusion seems to be consistent with the growing observational evidence for giant planets in binary star systems.

Because of the nature of a spherical coordinate grid, where  $\Delta x_{\phi} = r sin\theta \Delta \phi$  increases linearly with radius, the present models often fail to properly resolve any clumps that try to form near the edge of the edge. An improved treatment of disks being strongly perturbed by binary companions would require the use of adaptive mesh refinement (AMR) code or some other technique for better resolving clumps at large radii.

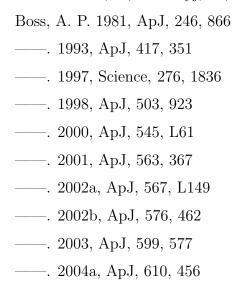
I thank Andy Nelson for details about the cooling times in his calculations, the referee for extremely helpful comments and questions about artificial viscosity and viscous dissipation, and Sandy Keiser for her continued expert assistance with the Carnegie Alpha Cluster. This research was supported in part by the NASA Planetary Geology and Geophysics Program under grant NNG05GH30G, by the NASA Origins of Solar Systems Program under grant NNG05GI10G, and by the NASA Astrobiology Institute under grant NCC2-1056. Calculations were performed on the Carnegie Alpha Cluster, the purchase of which was supported in part by NSF MRI grant AST-9976645.

#### REFERENCES

Barbieri, M., Marzari, F., & Scholl, H. 2002, A&A, 396, 219

Bodenheimer, P., Burkert, A., Klein, R. I., & Boss, A. P. 2000, in Protostars & Planets IV, ed. V. Mannings, A. P. Boss, & S. S. Russell (Tucson: Univ. Arizona Press), 675

Bodenheimer, P., Hubickyj, O., & Lissauer, J. J. 2000, Icarus, 143, 2



——. 2004b, ApJ, 616, 1265

——. 2005, ApJ, 629, 535

Boss, A. P., & Myhill, E. A. 1992, ApJS, 83, 311

Boss, A. P., & Yorke, H. W. 1993, ApJ, 411, L99

——. 1996, ApJ, 469, 366

Chambers, J. E., Quintana, E. V., Duncan, M. J., & Lissauer, J. J. 2002, AJ, 123, 2884

Chiang, E. I., et al. 2001, ApJ, 547, 1077

Chick, K. M., & Cassen, P. 1997, ApJ, 477, 398

Dartois, E., Dutrey, S., & Guilloteau, S. 2003, A&A, 399, 773

Dello Russo, N., et al. 2005, ApJ, 621, 537

Duquennoy, A., & Mayor, M. 1991, A&A, 248, 485

Eggenberger, A., Udry, S., & Mayor, M. 2004, A&A, 417, 353

Fischer, D. A., & Marcy, G. W. 1992, ApJ, 396, 178

Glassgold, A. E., Najita, J., & Igea, J. 2004, ApJ, 615, 972

Halbwachs, J. L., Mayor, M., & Udry, S. 2005, A&A, 431, 1129

Harten, A., & Zwas, G. 1972, J. Eng. Math., 6, 207

Hatzes, A. P., et al. 2003, ApJ, 599, 1383

Inaba, S., Wetherill, G. W., & Ikoma, M. 2003, Icarus, 166, 46

Kamp, I., & Dullemond, C. P. 2004, ApJ, 615, 991

Konacki, M. 2005, Nature, 436, 230

Kortenkamp, S. J., Wetherill, G. W., & Inaba, S. 2001, Science, 293, 1127

Larwood, J. D., Nelson, R. P., Papaloizou, J. C. B., & Terquem, C. 1996, MNRAS, 282, 597

Marzari, F., et al. 2005, ApJ, 618, 502

Marzari, F., & Scholl, H. 2000, ApJ, 543, 328

Mayor, M., et al, 2004, A&A, 415, 391

Mizuno, H. 1980, Prog. Theor. Phys., 64, 544

Mizuno, H., & Boss, A. P. 1985, Icarus, 63, 109

Moriwaki, K., & Nakagawa, Y. 2004, ApJ, 609, 1065

Mugrauer, M., et al. 2004, A&A, 425, 249

Myhill, E. A., & Boss, A. P. 1993, ApJS, 89, 345

Nelson, A. F. 2000, ApJ, 537, L65

Nelson, A. F., Benz, W., & Ruzmaikina, T. V. 2000, ApJ, 529, 357

Nelson, R. P. 2003, MNRAS, 345, 233

Notesco, G., & Bar-Nun, A. 2005, Icarus, 175, 546

Patience, J., et al. 2002, ApJ, 581, 654

Pickett, B. K., et al. 2000, ApJ, 529, 1034

Quintana, E. V., Lissauer, J. J., Chambers, J. E., & Duncan, M. J. 2002, ApJ, 576, 982

Rodríguez, L. F., et al. 1998, Nature, 393, 355

Thébault, P., et al. 2004, A&A, 427, 1097

Toomre, A. 1964, ApJ, 139, 1217

Tscharnuter, W. M., & Winkler, K.-H. 1979, Comput. Phys. Comm., 18, 171

Walker, G. A. H., et al. 1992, ApJ, 396, L91

——. 1995, Icarus, 116, 359

Zucker, S., et al. 2002, ApJ, 568, 363

This preprint was prepared with the AAS LATEX macros v5.2.

Fig. 1.— A copy of the paper that includes the figures may be downloaded from http://www.dtm.ciw.edu/boss/ftp/bin/.  $$_{24}$$ 

Table 1. Summary of disk instability models with and without binary companions.

model	$T_o$ (K)	$min(Q_i)$	$a_b$ (AU)	$e_b$	$\phi_{bi}$	$N_{\phi}$	$N_{Ylm}$	$t_f$ (yrs)
eb	40K	1.3	100	0.5	0	256	32	610
ab	50K	1.5	100	0.5	0	256	32	616
f	60K	1.6	-	_	_	256	32	1139
fb	60K	1.6	100	0.5	0	256	32	938
fbc	60K	1.6	50	0.5	0	256	32	831
fbca	60K	1.6	50	0.5	$\pi$	256	32	1126
g	70K	1.8	-	_	_	256	32	891
gbae	70K	1.8	100	0.25	$\pi$	256	32	616
gb	70K	1.8	100	0.5	0	256	32	1018
$_{ m gba}$	70K	1.8	100	0.5	$\pi$	256	32	1481
gbcae	70K	1.8	50	0.25	$\pi$	256	32	1059
gbca	70K	1.8	50	0.5	$\pi$	256	32	1146
gbcah	70K	1.8	50	0.5	$\pi$	512	48	630
gbc	70K	1.8	50	0.5	0	256	32	744
gbch	70K	1.8	50	0.5	0	512	48	429
h	80K	1.9	_	_	_	256	32	1970
hbae	80K	1.9	100	0.25	$\pi$	256	32	1903
hba	80K	1.9	100	0.5	$\pi$	256	32	1246
hbcae	80K	1.9	50	0.25	$\pi$	256	32	1910
hbca	80K	1.9	50	0.5	$\pi$	256	32	657